Biophysical Journal, Volume *122*

Supplemental information

Structural effects of spike protein D614G mutation in SARS-CoV-2

Hisham M. Dokainish and Yuji Sugita

Supporting Information of

Structural Effects of Spike Protein D614G Mutation in SARS-CoV-2

Hisham M. Dokainish[1] and Yuji Sugita[1,2,3,*]

[1]Computational Biophysics Research Team, RIKEN Center for Computational Science, 7-1-26 Minatojima-minamimachi, Chuo-ku, Kobe, Hyogo 650-0047, Japan

[2]Theoretical Molecular Science Laboratory, RIKEN Cluster for Pioneering Research, 2-1 Hirosawa, Wako, Saitama 351-0198, Japan

[3]Laboratory for Biomolecular Function Simulation, RIKEN Center for Biosystems Dynamics Research, 6-7-1 Minatojima-minamimachi, Chuo-ku, Kobe, Hyogo 650-0047, Japan

* Corresponding author (sugita@riken.jp)

Supplementary file includes:

Figure S1-S13

Table S1-S2

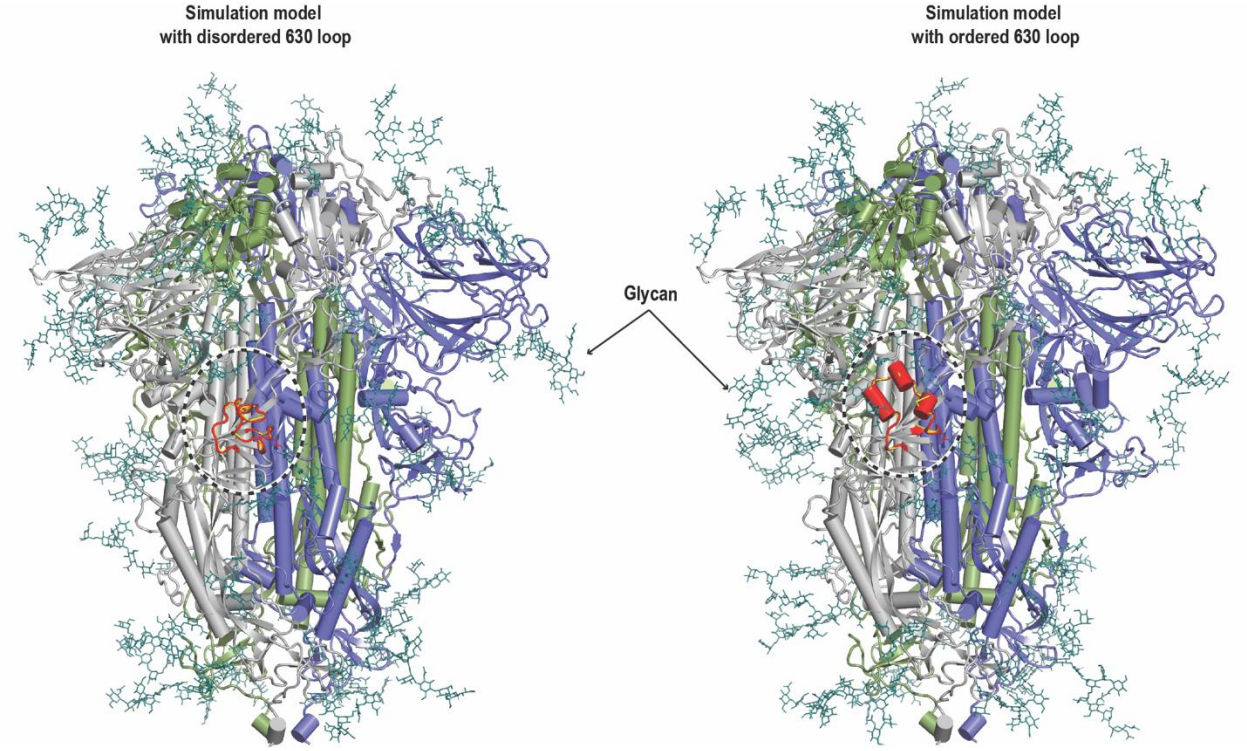

Figure S1. Cartoon representation of S-protein simulation models. Left: model of S-protein with disordered 630-loop based on PDB:6ZGE cryo-EM structures. Glycans were added in similar fashion to our previous study using the same list of Glycans. Right: Spike model with ordered 630-loop. The structure is also based on PDB:6ZGE while 630-loop structure was based on PDB:6XLU. Glycans are shown as deep teal sticks. The disordered 630-loop is shown in dark red and highlighted by dotted black circle.

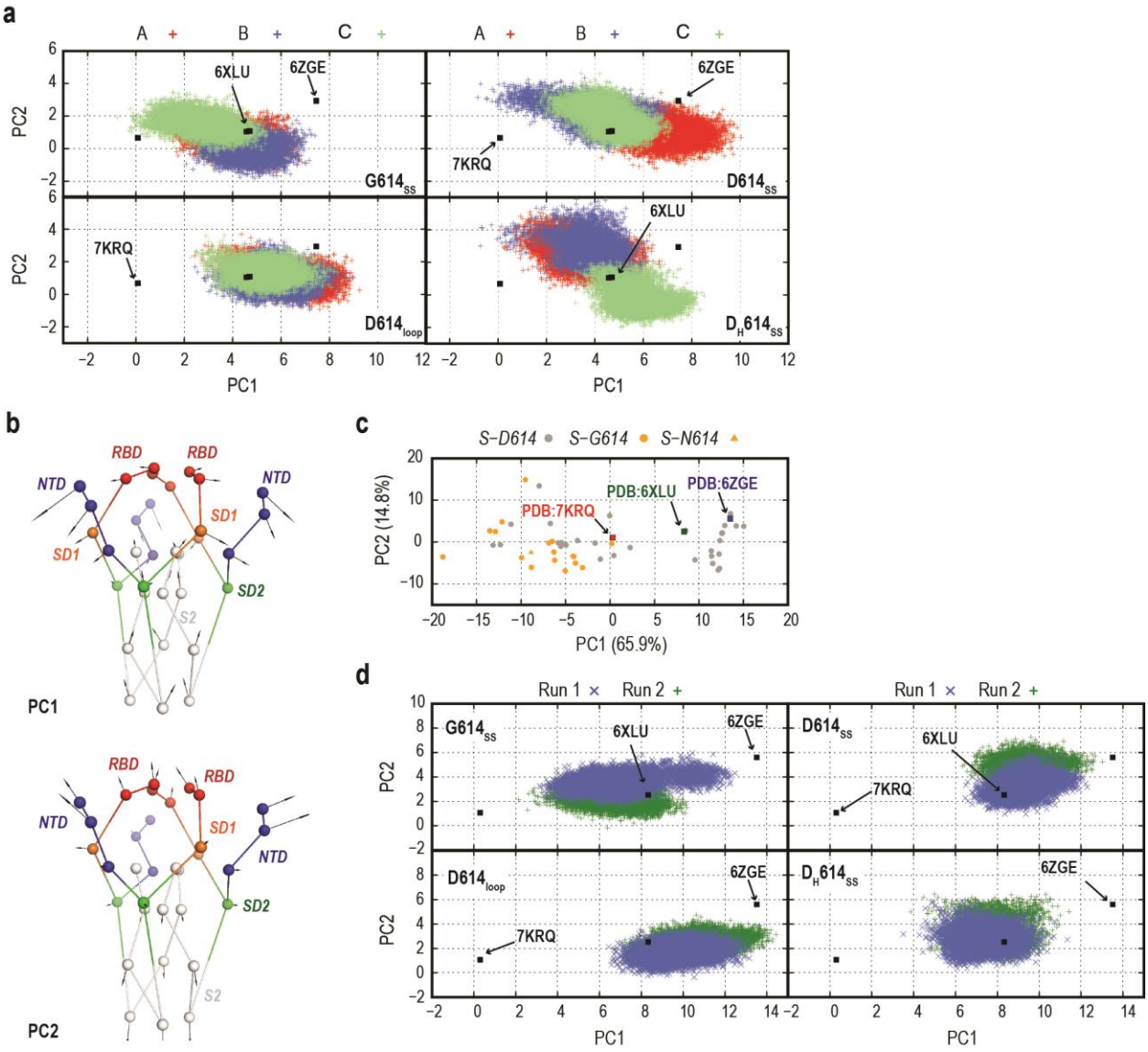

Figure S2. Trimeric 33 beads PCA analysis. a) Monomeric PCA projection of Run2 of all 4 systems. **b)** The lowest two modes (PC1 and PC2) from the 33 beads trimeric PCA of 52 cryo-EM structures. **c**) Projection of the 52 cryo-EM structure along PC1-PC2 space, where grey and orange represent D614 and G614 structures, respectively. Three important cryo-EM structures of wild type (PDB:6ZGE), wild type at pH 4 (PDB:6XLU) and D614G mutant (PDB:7KRQ) are shown as blue, green and red squares, respectively. **d**) Projections of all performed simulation snapshots using the 33-beads model. The two independent runs are shown in blue and green.

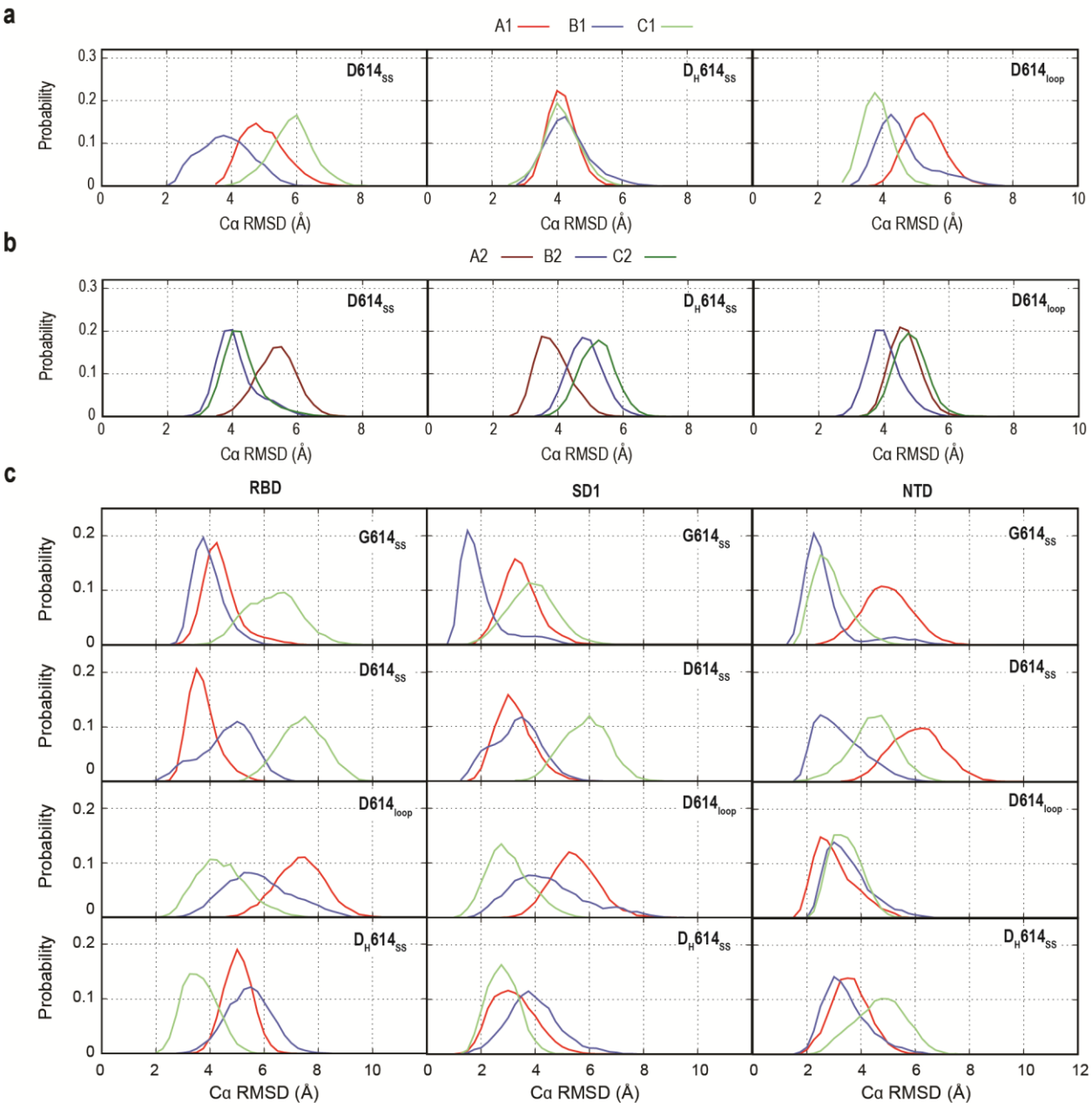

Figure S3. Domain RMSD analysis with respect to PDB:7KRQ. a) and b) Probability distributions of root mean square deviation (RMSD) of part of S1 (RBD, NTD and SD1) upon fitting S2 in all the three simulations starting from mutant spike structure for Run1 and Run2, respectively. **c)** Left, middle and right represent individual domains RMSD probabilities including RBD, SD1 and NTD, respectively. Top, middle top, middle bottom and bottom show the results from $G614_{SS}$, $D614_{SS}$, $D614_{loop}$ and D_H614_{SS}, respectively.

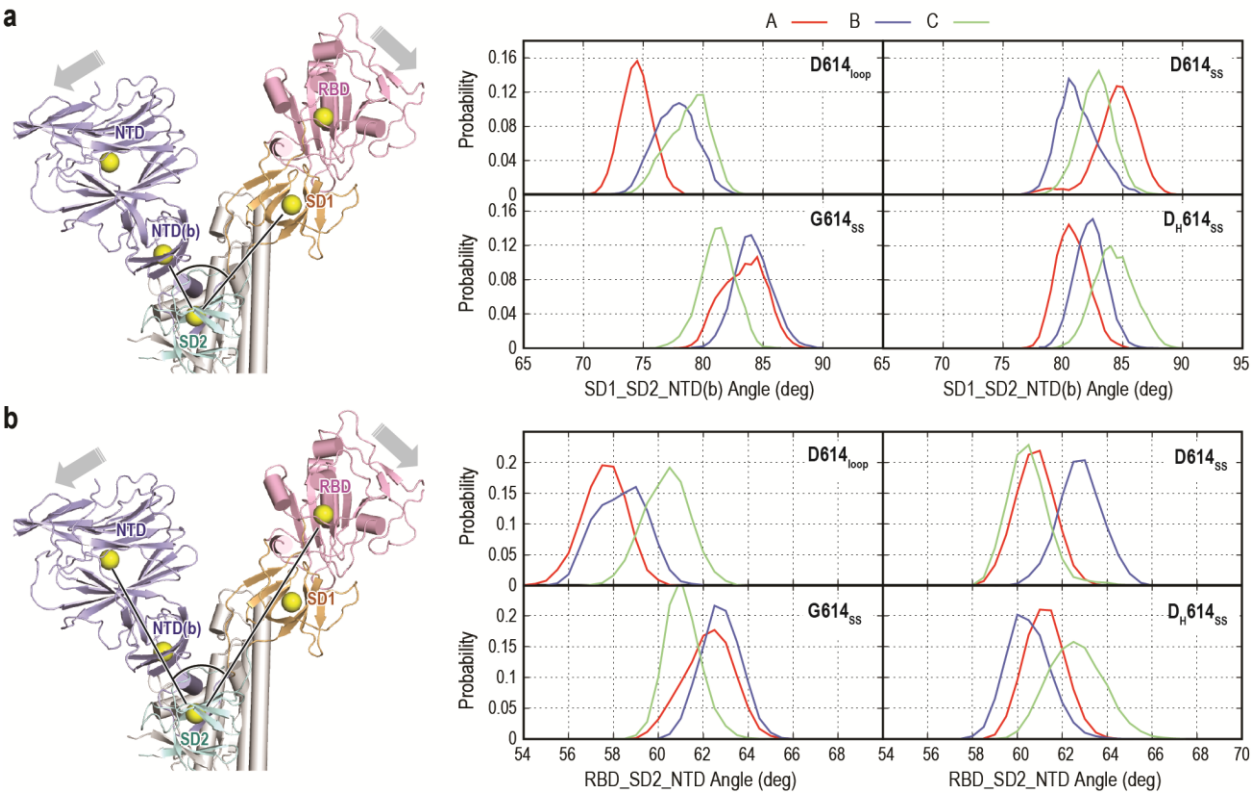

Figure S4. Structural changes in the interdomain angles upon the 630-loop rigidification. a) Angle formed between base of NTD (NDT(b)), SD2 and SD1 domains. **b**) Angle formed between RBD, SD2 and NTD. In both (a) and (b), Left: cartoon representation of S1 protomer is shown, where the center of mass of each domain are highlighted by yellow sphere representation. Right, probability distributions of the calculated angles.

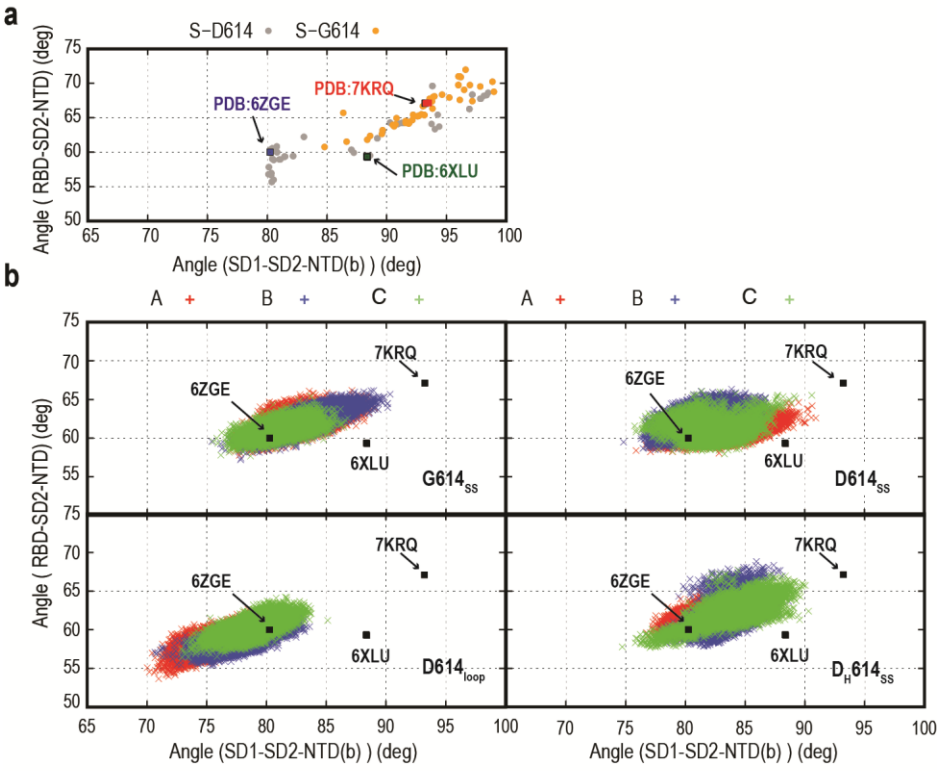

Figure S5. Interdomain angles in Cryo-EM structures and simulations. a) Distribution of interdomain angles in 156 protomers from Cryo-EM structures. **d**) Simulation interdomain angle distribution along main Cryo-EM structures of wild type and mutant (shown as black boxes).

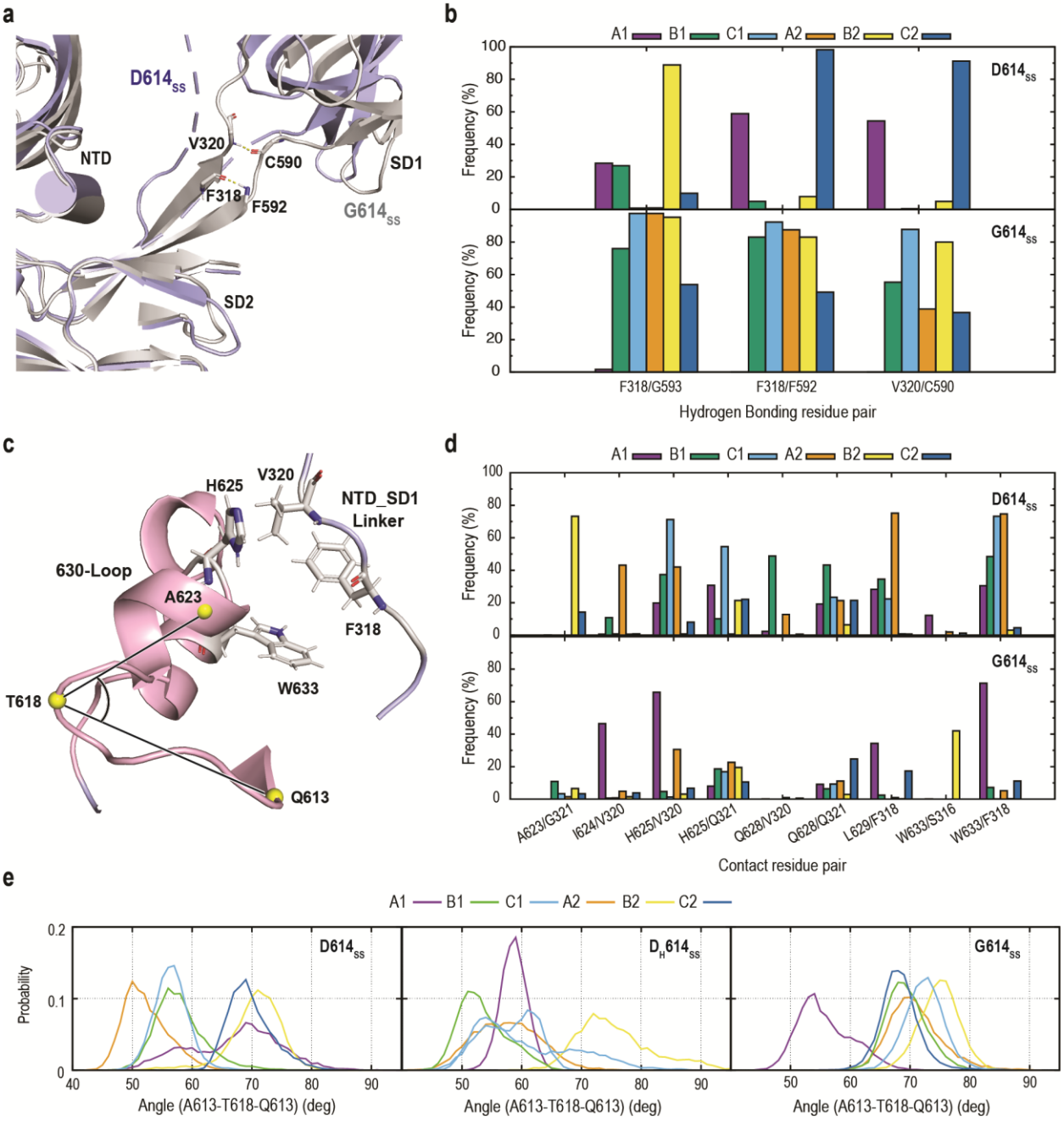

Figure S6. 630-loop insertion in G614ss vs D614ss. a) Cartoon representation of the linker regions connecting NTD to SD1 (residue 315to 321) and SD1 to SD2 (residue 590 to 595) of the last simulation structure in the two protomers that show conversion toward mutant structure projection in Figure 2 (protomer B in $G614_{SS}$ (grey) and $D614_{SS}$ (purple). Two backbone hydrogen bonding interactions are highlighted as yellow dotted line. **b)** Probability distributions of 3 linker regions backbone hydrogen boning interactions in $D614_{SS}$ (top) and $G614_{SS}$ (bottom). All 6 protomers of the two replicas per system are shown and indicated as A, B, C protomer, where 1 and 2 represent the replica number. **c)** Molecular representation of the 630-loop and NTD_SD1 linker hydrophobic interactions. Three Cα atoms are highlighted as yellow sphere, where the angle formed by them as shown as black line. **d)** Probability distribution of hydrophobic contacts between 630-loop and NTD_SD1 linker region. **e)** Probability distribution of the angle shown in (c) in all simulations with rigidified 630-loop.

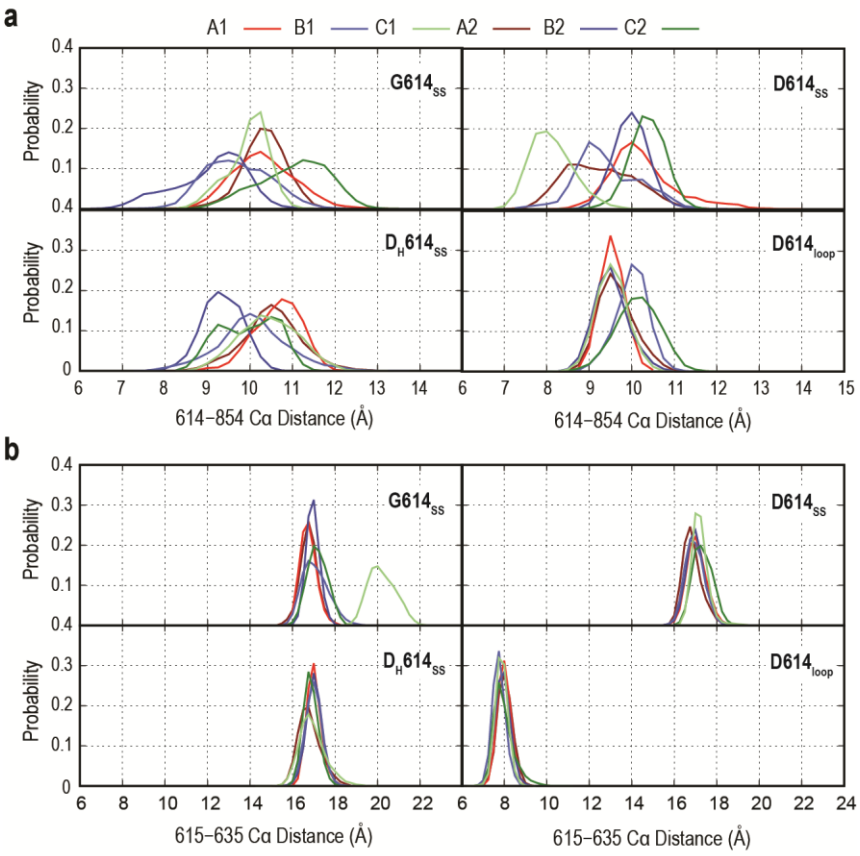

Figure S7. Changes in key inter-residue distances. Probability distribution of Cα distances between residues D614 (or G614) and K854 (**a**) and between residues V615 and V635 (**b**) in the four simulated systems,

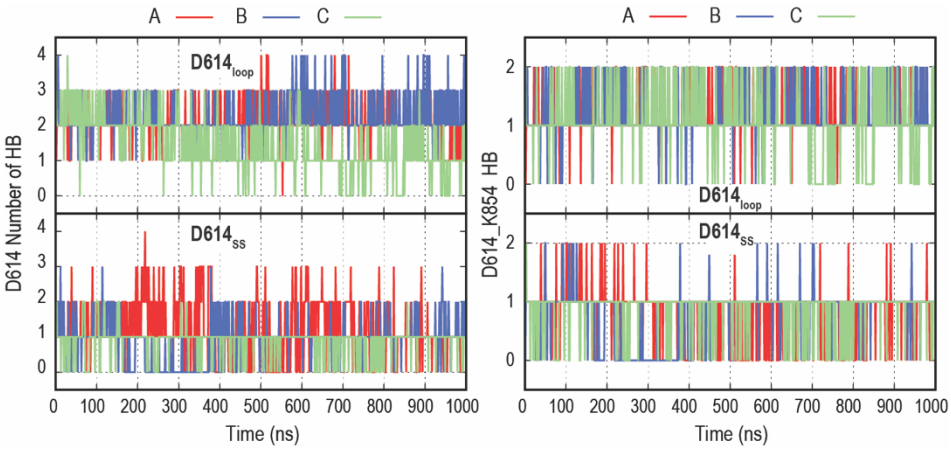

Figure S8. D614 Hydrogen bonding in Run2. Time series of D614 side chain total number of H-bonds (left), and D614/K854 salt bridge (right). Protomer are shown as A, B and C with red, blue and green colour, respectively. Top and bottom represent S-D614 with the ordered and disordered 630-loop, respectively.

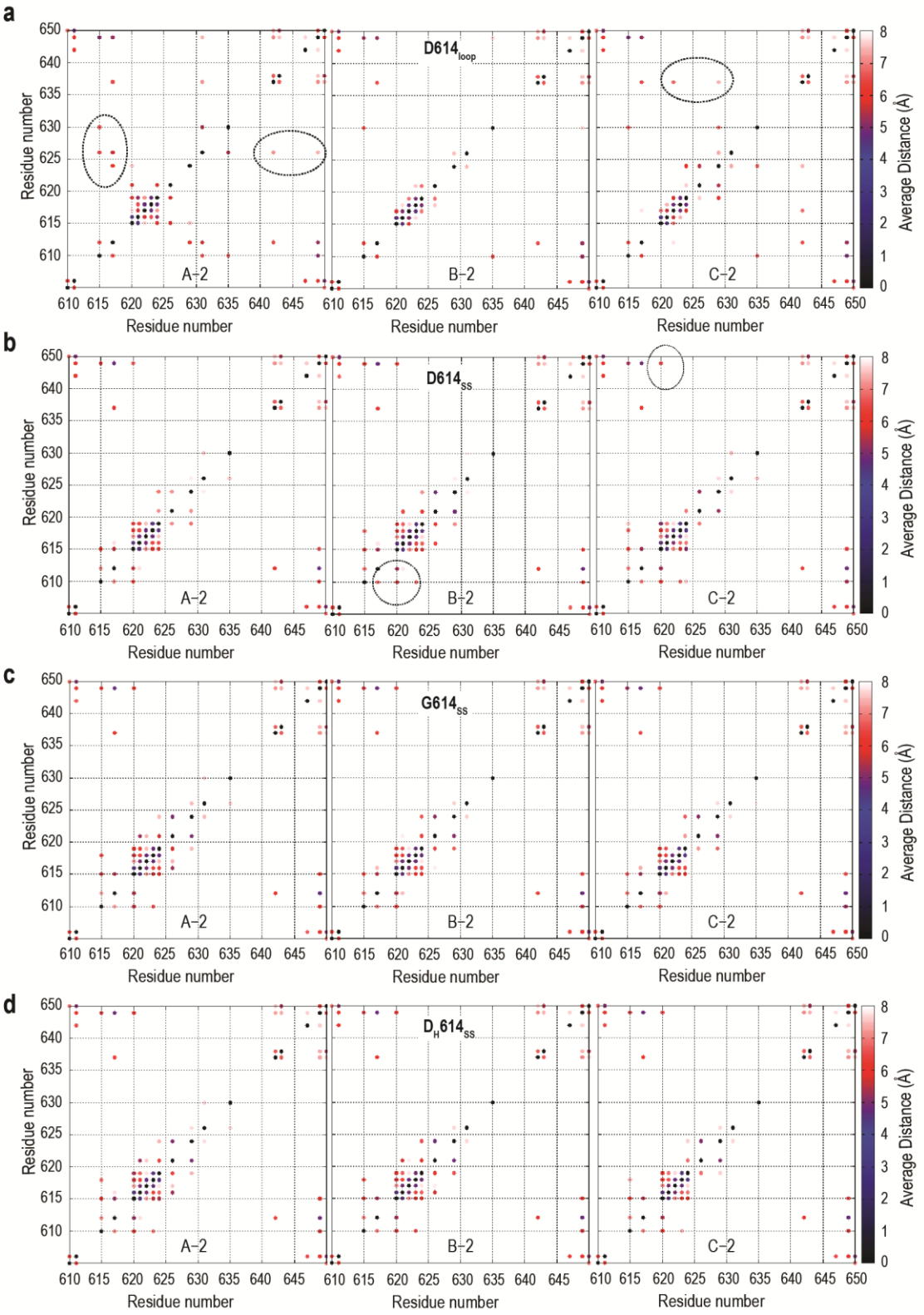

Figure S9. Hydrophobic contacts in 630-loop. Heatmap analysis of the average distance between hydrophobic residues in the 610-650 region.

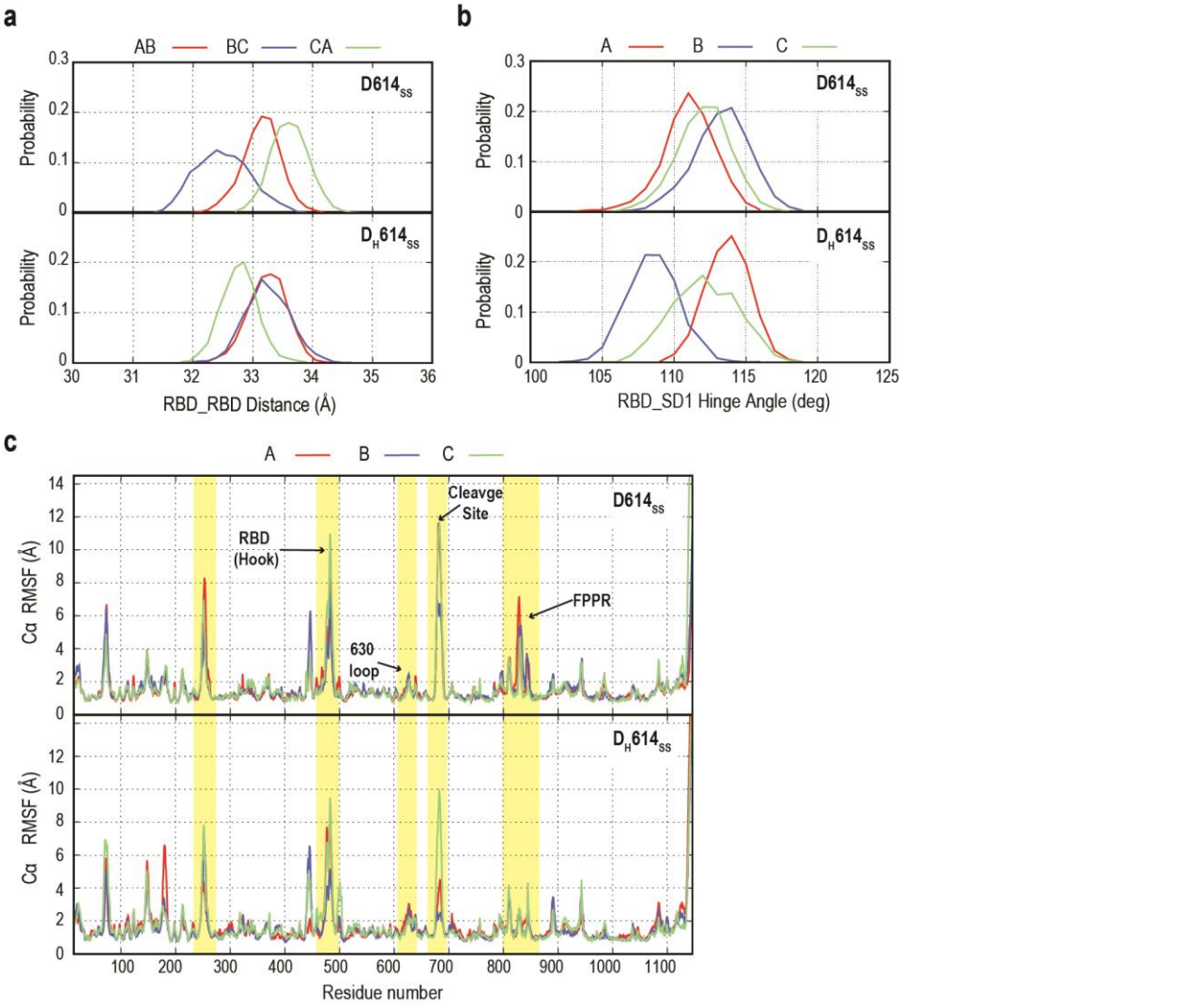

Figure S10. Stability of S-D614 in the presence of ordered loop with anionic and neutral Asp. a) Probability distribution of inter domain RBD distance (**a**) and RBD/SD1 hinge angle (**b**) in wild-type simulation with ordered 630-loop (D_H614_{SS} and $D614_{SS}$). **c**) Root mean square fluctuation of wild-type spike protomers in anionic ($D614_{SS}$) and neutral D614 (D_H614_{SS}) simulations.

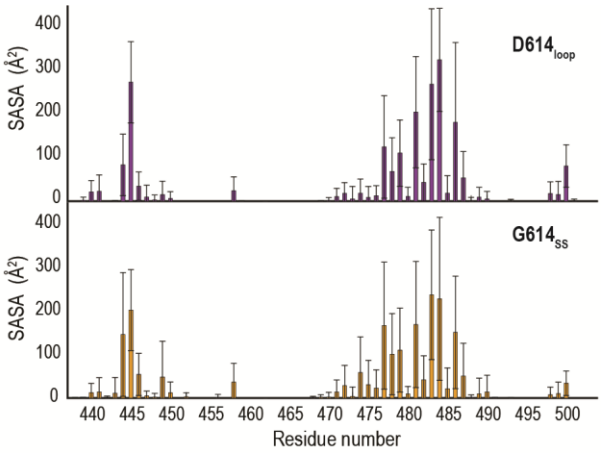

Figure S11. RBM in wild type vs mutant in the presence of glycans. Per residue solvent accessible surface area (SASA) analysis of RBD (RBM region) in the presence of glycans in $D614_{loop}$ and $G614_{SS}$.

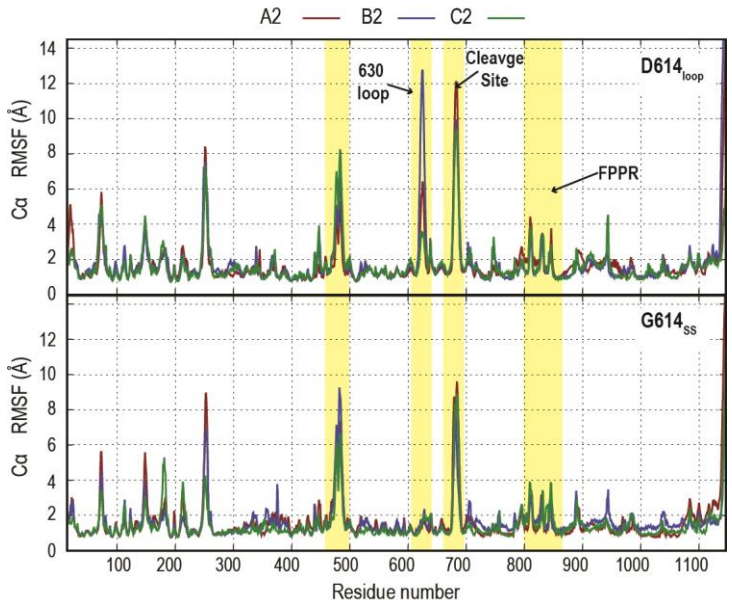

Figure S12. Root mean square fluctuation of wild-type spike protomers in anionic ($D614_{loop}$) and G614 ($G614_{SS}$) simulations from Run2.

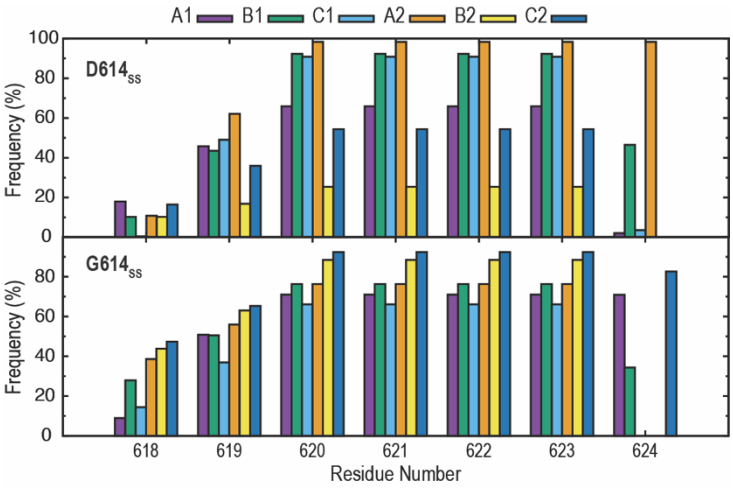

Figure S13. Individual frequency of α-helix in D614ss and G614ss. The α-helix in residues near to the mutation point (residue 618 to 624) in wild-type and mutant in the presence of rigidified 630-loo

Table 1. Cryo-EM structures used in the PCA.

PDB	Residue 614	PDB	Residue 614	PDB	Residue 614
6VXX	D614	6ZP2	D614	7KE8	G614
6X29	D614	6ZWV	G614	7KRQ	G614
6X2C	D614	7A4N	N614	7L7K	D614
6X6P	D614	7BNM	G614	7LWI	G614
6X79	D614	7CAB	D614	7LWJ	G614
6XF5	D614	7DDD	D614	7LWK	G614
6XLU	D614	7DF3	D614	7LWL	G614
6XM5	D614	7DWY	D614	7LWS	G614
6XR8	D614	7E7B	D614	7LYL	G614
6ZB4	D614	7E7D	D614	7LYM	G614
6ZB5	D614	7JJI	D614	7M0J	D614
6ZGE	D614	7JWY	D614	7N1T	G614
6ZGI	D614	7KDG	D614	7N1U	G614
6ZOX	D614	7KDI	G614	7NT9	D614
6ZOY	D614	7KDK	G614	7JJJ	D614
6ZOZ	D614	7KE4	G614	7JJJ	D614
6ZP0	D614	7KE6	G614		
6ZP1	D614	7KE7	G614		

Table 2. Definition of protomer coarse-grained particles representing rigid domains for PCA.

Bead	Residue Number
NTD’	44-53, 272-293
NTD	27-43, 54-271
NTD(b)	116-119, 169-172
RBD	330-443, 503-528
RBD’	403-410
SD1	323-329, 529-590
SD2	294-322, 591-696
S2(1)	717-727, 1047-1071
S2(2)	711-716, 1072-1122
S2(3)	769-772, 1011-1014
S2(4)	740-743, 964-967, 999-1002